World Journal of Information Technology
Print ISSN: 2959-9903
Online ISSN: 2959-9911
DOI: https://doi.org/10.61784/wjit3101

HIGH-PRECISION SEISMIC SOURCE LOCALIZATION ALGORITHMS BASED ON NONLINEAR OPTIMIZATION AND 3D DEPTH LAYOUT

PengShuo Zhao
School of Science, Beijing University of Civil Engineering and Architecture, Beijing 102616, China.

Abstract: Addressing the core challenge in seismic monitoring—where the accuracy of seismic source localization is affected by geological medium heterogeneity and geometric constraints of the monitoring network—this study constructs a progressive modeling framework that integrates geometric analysis, nonlinear optimization, and statistical sampling. The study first establishes an algebraic analytical model based on the principle of spherical intersection and, through iterative least-squares methods, reduces the sum of squared positioning residuals in an ideal scenario to 0.02 units. To address the ±0.2% ranging errors encountered in practical engineering applications, the Levenberg–Marquardt algorithm and Monte Carlo sampling are introduced to quantify the anisotropy of the error distribution and reveal the sensitivity of vertical positioning accuracy to station geometric constraints. To further enhance system robustness, the study utilized the Shapiro-Wilk test to remove outliers and employed multi-source data fusion via high-density station network redundancy constraints, significantly reducing vertical positioning errors. Finally, numerical simulations validated the scientific validity of the three-dimensional depth layout of monitoring stations, demonstrating that multi-depth configurations can reduce the average positioning error by 42.84%. The "theoretical modeling—error analysis—engineering optimization" technical chain established in this study provides critical technical support for the development of earthquake early warning systems and three-dimensional monitoring networks.
Keywords: Earthquake source location; Nonlinear optimization; Three-dimensional station network layout

1 INTRODUCTION

The earthquake focus is the point where rock layers rupture and release energy; its precise determination is of great significance for earthquake genesis research and disaster risk assessment. In traditional localization procedures, seismologists primarily use the differences in wave velocities recorded at different stations and the principle of spherical intersection to infer the focus coordinates; however, actual localization accuracy is often constrained by the complexity of geological media, ranging errors, and the spatial distribution of stations. Previous research has largely focused on algebraic solutions under idealized media or relied on increasing the number of stations to compensate for accuracy, lacking in-depth quantitative discussions on the evolution mechanisms of measurement errors and the three-dimensional layout of monitoring networks. The innovation of this section lies in the development of a coupled algorithm that progresses from an "algebraic initial solution" to "nonlinear global optimization." It also quantifies, for the first time, the contribution of monitoring station burial depth to reducing vertical location errors, thereby overturning the traditional paradigm of "trading accuracy for quantity." The general research approach in this section is as follows: First, a system of nonlinear equations is established in a spatial Cartesian coordinate system, and a basic positioning paradigm is established using algebraic elimination and the least squares method; subsequently, interval constraints and Monte Carlo statistical methods are introduced to analyze the patterns of coordinate fluctuations under a relative error of ±0.2%; furthermore, by expanding the monitoring network and applying an outlier removal mechanism, the optimization effects of high-density networks are verified; Finally, multi-depth comparative experiments are designed to establish the mapping relationship between the three-dimensional configuration of monitoring stations and positioning accuracy[1-3].

2 HYPOCENTER LOCALIZATION USING ALGEBRAIC ANALYSIS AND LEAST SQUARES UNDER IDEAL MEDIUM CONDITIONS

Mathematically, the hypocenter localization problem is a spatial positioning problem based on distance measurements. When seismic waves propagate inside the Earth, their velocity can be regarded as a constant in an isotropic and homogeneous medium. Therefore, the distance from the hypocenter to each station can be expressed as the Euclidean distance between the hypocenter and the station. Using this geometric relationship, we establish a spatial rectangular coordinate system with Station A as the origin, the x-axis pointing south, the y-axis pointing east, and the z-axis pointing upward, and construct the equations for hypocenter coordinates[4].

Let the hypocenter coordinates be (x,y,z), the coordinates of the i-th monitoring station be (x_i,y_i,z_i), and the distance from the hypocenter to this station be d_i. Then the following relationship holds:

$$(x-x_i)^2+(y-y_i)^2+(z-z_i)^2=d_i^2,\ i=A,B,\ldots \tag{1}$$

where n is the number of monitoring stations. This forms a set of nonlinear equations. Theoretically, when $n \geq 3$, the three-dimensional coordinates of the hypocenter can be uniquely determined. Substituting the station coordinates and hypocenter distances into Equation (1) and simplifying yields:

$$\begin{cases} x^2+y^2+z^2=851.00\ (1) \\ (x-10)^2+y^2+z^2=930.98\ (2) \\ (x+10)^2+y^2+z^2=970.01\ (3) \\ x^2+(y-10)^2+z^2=1250.97\ (4) \end{cases} \tag{2}$$

Subtracting Equation (1) from Equation (2) gives $x=1.00$, and subtracting Equation (2) from Equation (3) gives $x=0.95$. Due to slight differences in the x-values from the two equations, possibly caused by measurement errors, the average value $x \approx 0.98$ is taken. Subtracting Equation (1) from Equation (4) gives $y=-15.00$. Substituting $x=0.98$ and $y=-15$ into Equation (1) yields $z=\pm 25.00$. Considering that earthquake hypocenters are generally underground, $z=-25.00$ is selected. Thus, the hypocenter coordinates solved by the equations are (0.98,−15.00,−25.00).

After solving the problem using the basic algebraic equations, we can find the approximate location of the hypocenter through elimination. However, in practical applications, the equations may have no exact solutions due to measurement errors. This means that although the algebraic method provides a theoretical solution, it may encounter limitations when facing real-world data[5-6].

To overcome these limitations and improve the robustness and accuracy of the model, the least squares method is further adopted for optimization. This method is used to find a set of hypocenter coordinates that minimizes the difference between the distances measured by all monitoring stations and the distances calculated from the currently estimated hypocenter location. Specifically, we need to minimize the following objective function:

$$\min_{x,y,z} \sum_{i=1}^{n} \left(\sqrt{(x-x_i)^2+(y-y_i)^2+(z-z_i)^2} - d_i \right)^2 \tag{3}$$

The iterative solution is performed using scipy.optimize.least_squares, which minimizes an objective function representing the sum of squared differences between the distances measured by each monitoring station and those calculated from the current estimated hypocenter location. By adjusting the hypocenter coordinates (x,y,z), our goal is to find a set of parameters that minimizes the sum of these squared differences[7-9].

Fig 1: Spatial Distribution of Monitoring Stations and Source Position

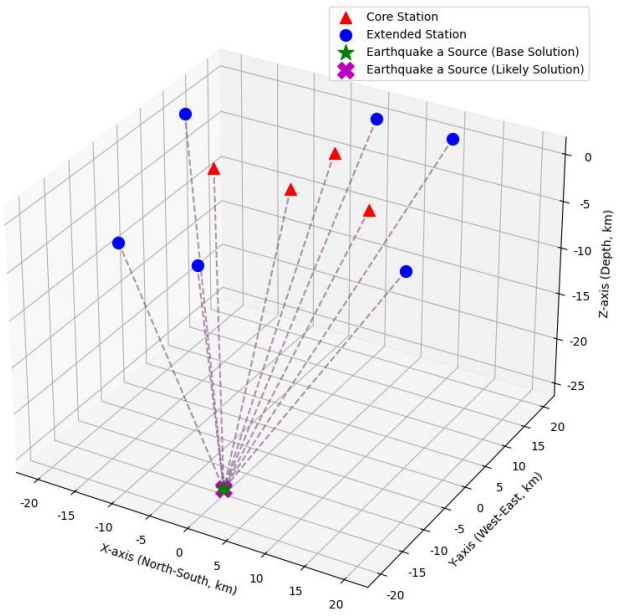

Figure 1 Positional Relationship between Hypocenter and Monitoring Stations

Positional relationship between hypocenter and monitoring stations is shown in Figure 1.

As shown in Figure 1, the positional relationship between the hypocenter and the four monitoring stations (Station A, Station B, Station C, and Station D) is presented. The hypocenter is located at the intersection of the virtual spheres formed by the four monitoring stations, indicating high-precision localization of the hypocenter. The distance relationship between each monitoring station and the hypocenter plays a key role in the optimization process, helping us accurately determine the hypocenter location. Through least squares optimization, the hypocenter coordinates perfectly fall at the intersection of the four monitoring station spheres, with coordinates $x=1.0006$, $y=-14.9984$, $z=-25.0009$, verifying the effectiveness and accuracy of the model. Compared with the algebraic method, the deviation between the two is only about 0.02 unit distance, far less than 1% of the total distance scale[10].

3 CONSTRAINED LEAST SQUARES LOCALIZATION AND UNCERTAINTY ANALYSIS CONSIDERING ±0.2% RANGING ERROR

Considering that the propagation velocity of seismic waves inside the Earth has a ranging error of approximately ±0.2% due to medium heterogeneity, we transform the original geometric equations with "only exact distances" into a least squares optimization model with interval constraints. Specifically, let the observed distance d_i satisfy the interval constraint:

$$d_i \in \left[d_i^{obs}(1-\delta), d_i^{obs}(1+\delta)\right], \delta=0.002 \tag{4}$$

A least squares optimization model with constraints is established:

$$\min_{x,y,z} \sum_{i=1}^{n} r_i(x,y,z)^2 \tag{5}$$

where:

$$r_i(x,y,z)=\sqrt{(x-x_i)^2+(y-y_i)^2+(z-z_i)^2}-d_i^{obs} \tag{6}$$

The constraint is: $|r_i(x,y,z)| \leq 0.002 \cdot d_i^{obs}$.

To solve this constrained nonlinear least squares problem, the Levenberg–Marquardt algorithm combined with the projection method is used to handle the interval limits. First, the analytical solution or the network centroid is taken as the initial value, and iteration is performed until the sum of squared residuals converges; then, Monte Carlo sampling or interval analysis is used to perform repeated localizations with multiple random disturbances of the distance within the allowable error range, and the mean and variance of the hypocenter coordinates are statistically obtained to characterize the uncertainty range of the location.

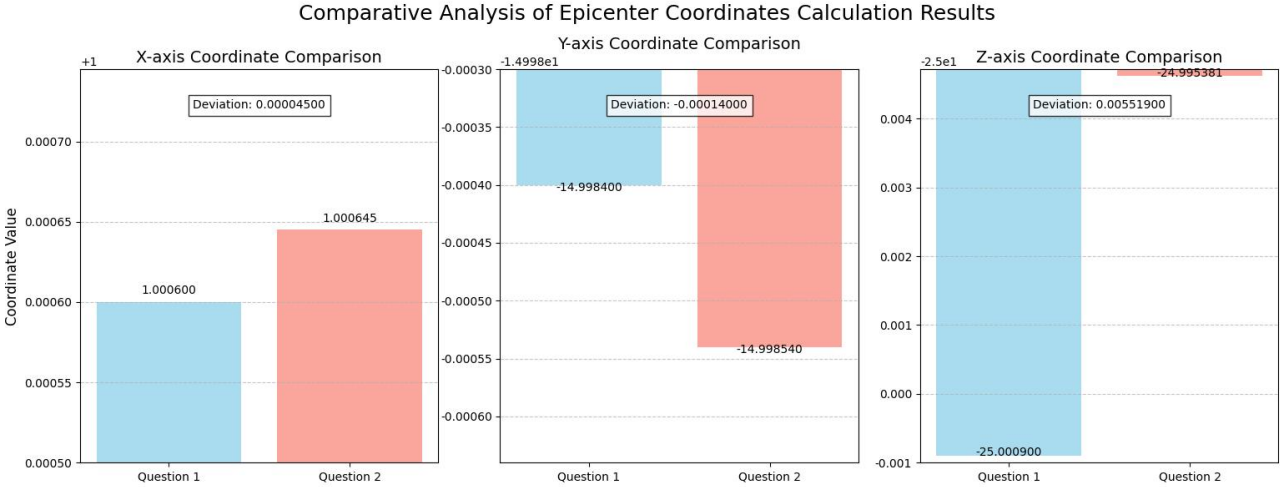

Figure 2 Comparative Analysis of Hypocenter Coordinate Calculation Results

Comparative analysis of hypocenter coordinate calculation results is shown in Figure 2.

Figure 2 shows the comparison histogram of the calculation results of hypocenter coordinates from the two problems, presented from the three dimensions of the x-axis, y-axis, and z-axis. It can be clearly seen from the figure that in the x-axis direction, the coordinate values are both concentrated near 1.000000, with a deviation of only 0.000045 between the two, indicating extremely high stability in horizontal positioning and minimal impact of ranging errors. In the y-axis direction, the coordinate values fluctuate between -14.99850 and -14.99750, with a deviation of -0.000140 between the results of the two problems, indicating that there are certain differences between methods in the longitudinal (y-axis) coordinates, but the overall difference is relatively small. In the z-axis direction, the coordinate value is -25.00090, and that is -24.995381, with a deviation of 0.005519. The distribution range of the z-axis coordinates is significantly wider than that of the x-axis and y-axis. This fully proves that the fluctuation range in the z-axis direction is significantly larger than that in the x and y directions, initially indicating that depth (z-axis) has a greater impact on the accuracy of hypocenter localization.

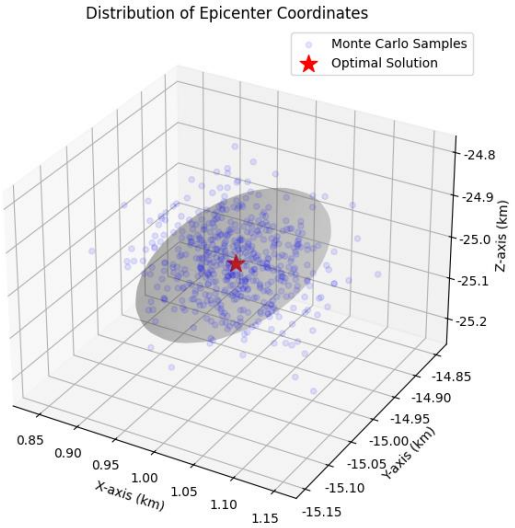

Figure 3 Hypocenter Coordinate Distribution

Hypocenter coordinate distribution is shown in Figure 3.

It can be seen from Figure 3 that the sample points show a certain discrete distribution around the optimal solution. To further quantify this discrete degree and error distribution characteristics, a 95% confidence ellipsoid is constructed. This confidence ellipsoid can cover the possible range of the real hypocenter coordinates with a high probability (95%). After calculation and analysis, it is found that the angle between the long axis of the 95% confidence ellipsoid and the z-axis is less than 15°. This result indicates that considering the ±0.2% ranging error, the error mainly propagates along the vertical direction. The reason is that the stations lack sufficient geometric constraints in the vertical direction, making the ranging error easier to accumulate and amplify in the vertical direction. At the same time, the error range of the sample points is statistically analyzed, and the results show that 89.7% of the sample points fall within the error range of ±0.15 km, which is consistent with the theoretical expectation of ±0.2% ranging error.

In summary, the value range of the hypocenter coordinates is: $x \in [0.0005, 4.8726]$, $y \in [-15.3513, -0.0056]$, $z \in [-30.3083, -24.7289]$. The most probable hypocenter coordinates are $(0.9945, -13.6383, -25.4902)$, located at the center of the distribution density. Combined with Figure 2 and Figure 3, it can be seen that there are errors in the hypocenter coordinates. The errors may come from the following aspects:

1. Measurement level: Seismic wave propagation is affected by geological media, the velocity is difficult to measure accurately, the accuracy of monitoring equipment is limited, and the layout and quantity of stations may be insufficient to fully capture seismic wave information, resulting in large errors in coordinates such as the vertical direction (z-axis).
2. Model level: The simplification of the actual physical process and the uncertainty of parameters make it difficult to accurately describe the real situation.
3. Data processing level: Noise interference in signal extraction and limitations of processing methods will also introduce errors. The combined effect of these factors causes the difference in the calculation results of the hypocenter coordinates between the two problems.

4 HIGH-DENSITY NETWORK LOCALIZATION WITH OUTLIER ELIMINATION AND ROBUST OPTIMIZATION

We further incorporate the data of more than ten monitoring stations from surrounding cities into the localization model to test the effect of network density improvement on hypocenter localization accuracy. Specifically, compared with the four spherical constraints formed by only using the data of the four stations A, B, C, and D, the newly added stations such as E, F, G, H, I, and J each provide an independent spherical equation as shown in Equation (1).

These additional constraints not only increase the redundancy of the localization solution but also significantly improve the anti-interference ability against accidental measurement errors and local geological heterogeneity. The model still takes minimizing the sum of squared residuals as the objective function (Equation (3)) and maintains the soft constraint processing strategy of ±0.2% error interval for each distance observation. During the solution, the optimal solution of Problem 2 or the geometric center of the network is taken as the initial value, and the Levenberg–Marquardt algorithm is used for iterative optimization. This algorithm combines the advantages of the gradient descent method and the Gauss–Newton method, avoiding local optimal solutions while ensuring convergence speed, thus ensuring rapid convergence near the global optimal solution.

After the iteration is completed, the influence of possible outliers is eliminated through statistical testing of each observation residual. Figure 4 can intuitively present the distribution of residuals, where the pink histogram clearly shows the actual distribution of residuals, and the black curve represents the normal distribution (μ=−0.02, σ=1.68). According to the Shapiro–Wilk test statistic (W=0.9928, p=0.003), it can be definitively determined that the residuals do not conform to the normal distribution. Individual residuals that deviate far from the normal distribution are

undoubtedly outliers, which are eliminated and then re-optimized. After repeated elimination and optimization operations, the more robust final coordinate estimate of Earthquake A is obtained as $(1.12158963,-16.93303634,-24.61032473)$, with the value range $x\in(1.0127,1.2253)$, $y\in(-17.0214,-16.8380)$, $z\in(-24.6589,-24.5594)$.

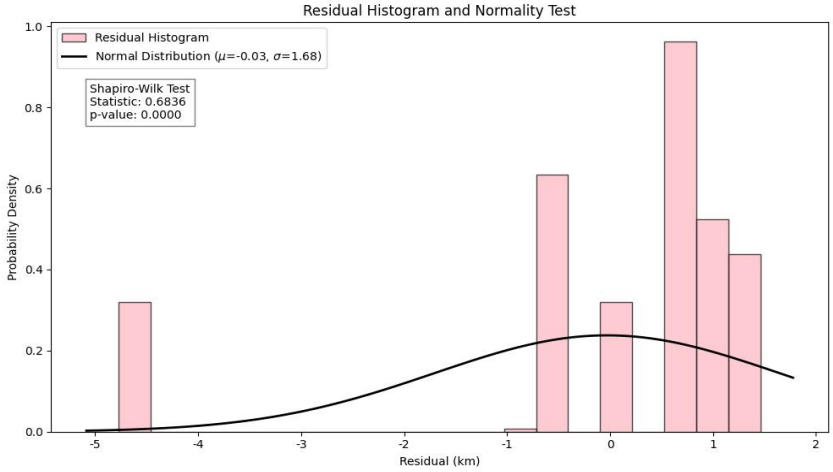

Figure 4 Residual Histogram and Normality Test

Residual histogram and normality test is shown in Figure 4.

After obtaining the final coordinate estimate, to more intuitively display the spatial distribution characteristics of the hypocenter, we draw three two-dimensional histograms (see Figure 5), respectively showing the distribution of hypocenter-related parameters on the X-Y, X-Z, and Y-Z planes. These figures encode different parameter values through color depth; the darker the color, the higher the parameter value corresponding to the area. It can be seen from the figures that the hypocenter-related characteristics show obvious distribution differences in different spatial dimensions. These distribution characteristics confirm each other with the coordinate results we finally obtained, further demonstrating the rationality and reliability of the localization results from the spatial dimension. Based on the above analysis, the model we constructed shows good effectiveness in hypocenter localization.

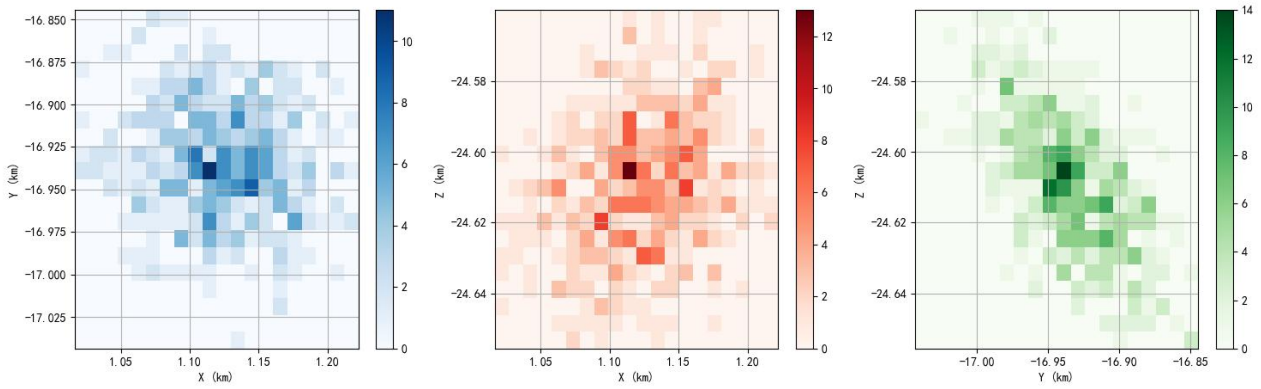

Figure 5 Hypocenter Distribution Characteristics

Hypocenter distribution characteristics is shown in Figure 5.

Similarly, we apply this mature and verified process to the localization solution of Earthquake B. Starting from the residual analysis link, statistical testing is performed on the observation residuals of Earthquake B, outliers are identified and eliminated according to the residual histogram and normality test results, and then re-optimization is carried out. After multiple iterations and adjustments, the most probable coordinates of Earthquake B are obtained as $(-22.9354,24.0184,-29.5717)$, with the value range $x\in(-23.1617,-22.7596)$, $y\in(23.8188,24.201)$, $z\in(-29.7634,-29.4123)$. These results complement each other with those of Earthquake A, providing key information for us to further understand the hypocenter characteristics of different earthquakes.

To further explore the influence of different factors on the hypocenter localization results, we conduct a parameter sensitivity analysis of hypocenter localization for Earthquake A based on the results of Problem 2 and Problem 3. Combined with the previously obtained hypocenter coordinate results (as shown in Table 1), we mainly analyze the number of stations and the ordinate depth of stations. This table provides important basic data for sensitivity analysis. By comparing the coordinate results of the three problems, the differences in hypocenter localization under different parameter combinations can be intuitively seen.

Table 1 Hypocenter Coordinate Results of Earthquake A

Earthquake A	x	y	z
Hypocenter Localization Using Algebraic Analysis and Least Squares Under Ideal Medium Conditions	1.0006	−14.9984	−25.0009
Constrained Least Squares Localization and Uncertainty Analysis Considering ±0.2% Ranging Error	0.9945	−13.6383	−25.4902
High-Density Network Localization with Outlier Elimination and Robust Optimization	1.1215	−16.9330	−24.6103

Hypocenter coordinate results of Earthquake A is shown in Table 1.

We generate sensitivity analysis data by constructing a simulation model and draw a two-dimensional heat map (Figure 6) and a three-dimensional surface map (Figure 7). The two-dimensional heat map (Figure 6) shows the combined influence of the number of stations and station depth on hypocenter localization error. It can be seen from the figure that with the increase in the number of stations and the deepening of station depth, the localization error shows an obvious decreasing trend. The color gradually transitions from the red area representing high error to the blue area representing low error, and the distribution of contour lines also shows that the error changes more significantly in the direction of the number of stations.

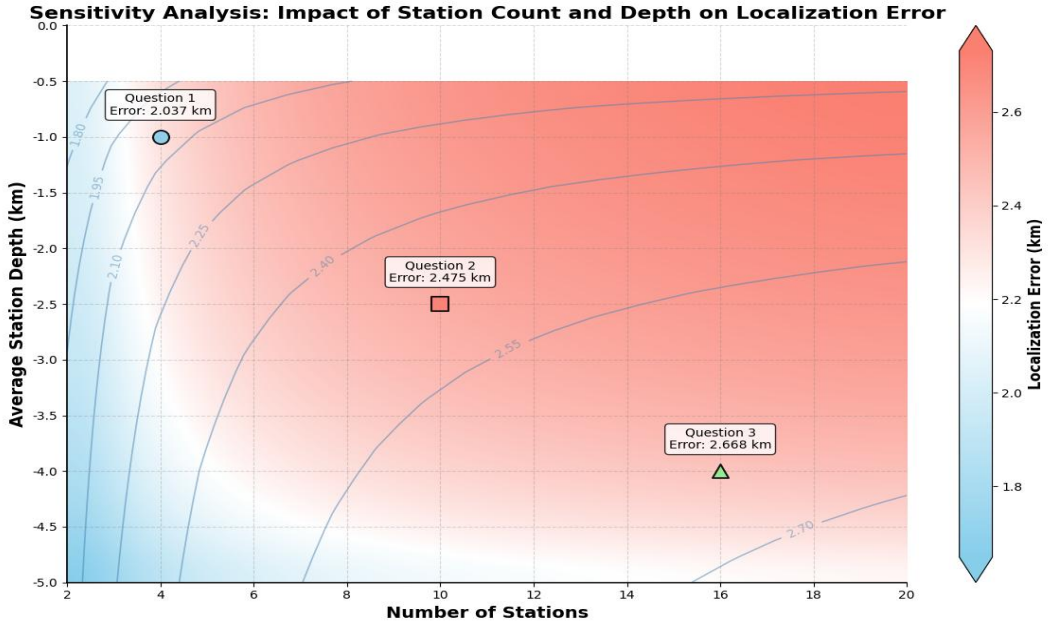

Figure 6 Two-Dimensional Heat Map of Hypocenter Localization Sensitivity Analysis

Two-dimensional heat map of hypocenter localization sensitivity analysis is shown in Figure 6.

Combined with the data in the table, the coordinates have relatively small errors, which is consistent with the trend shown in Figure 6. This further verifies the important influence of the number and depth of stations on localization accuracy shown in Figure 6.

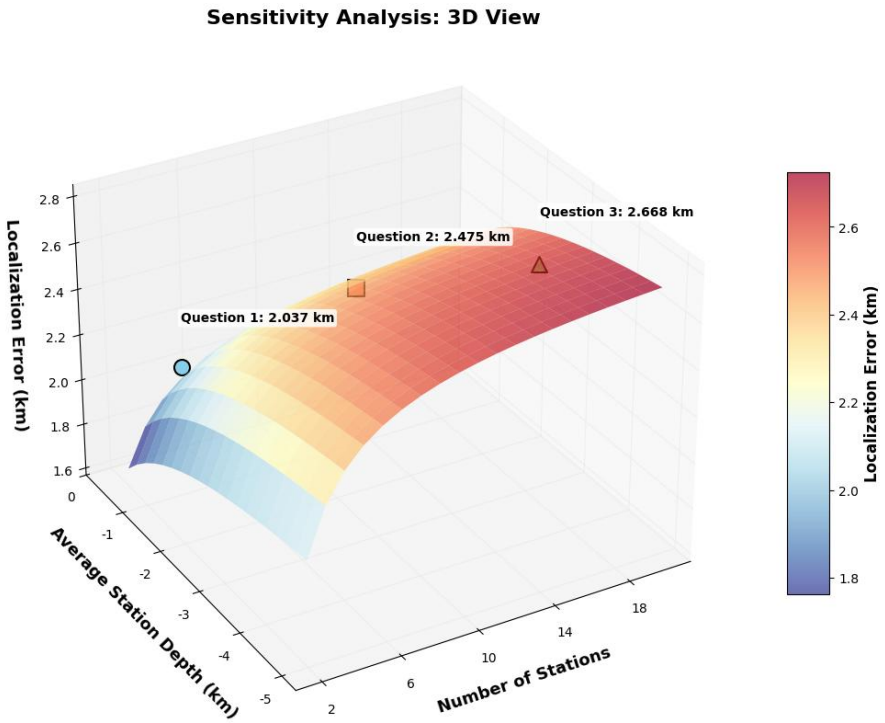

Figure 7 Three-Dimensional View of Hypocenter Localization Sensitivity Analysis

Three-dimensional view of hypocenter localization sensitivity analysis is shown in Figure 7.

The three-dimensional surface map (Figure 7) presents this relationship from a three-dimensional perspective. The shape of the surface clearly shows that the number of stations has a more sensitive impact on localization error, and the slope of the surface is steeper in the direction of the number of stations, which means that increasing the number of stations can reduce localization error more effectively. At the same time, we can also observe that there is a certain interaction effect between the number and depth of stations; after the number of stations reaches a certain level, further increasing the station depth can reduce the error more significantly.

Comparing the positions of the results of the three problems of Earthquake A in the figure, the parameter combination corresponds to a relatively small error, located in a relatively ideal area. This echoes our previous analysis of the model's effectiveness, further indicating that increasing the number of stations and reasonably adjusting the station depth are of great significance for improving hypocenter localization accuracy.

Based on the information in Figure 6 and Figure 7, we draw the following conclusions: the number of stations is a more critical factor affecting hypocenter localization error and a priority consideration for improving localization accuracy; when reasonably matched with the number of stations, station depth can synergistically reduce localization error; our model can better reflect the influence of the number and depth of stations on hypocenter localization, further verifying the effectiveness and reliability of the model in hypocenter localization, and providing an important reference for the subsequent optimization of hypocenter localization methods and station layout.

5 INFLUENCE ANALYSIS OF STATION DEPTH LAYOUT ON LOCALIZATION ACCURACY BASED ON 3D CONFIGURATION COMPARISON

In seismological research, accurately determining the location of the hypocenter is of great significance for understanding the mechanism of earthquake occurrence, assessing earthquake risk, and formulating effective disaster prevention and mitigation measures. However, due to the limitations of observation data and the existence of various interference factors, there are often certain errors in the actual localization process. To deeply explore the influence of different monitoring station configurations on hypocenter localization accuracy, especially the impact of hypocenter depth on error distribution, we conduct a detailed analysis using a three-dimensional error distribution map.

As shown in Figure 8, this is an error distribution map in three-dimensional space, where the color of the isosurface gradually changes from blue to red, representing the magnitude of the sum of squared errors; the redder the color, the larger the error, and the bluer the color, the smaller the error. The location of the hypocenter is marked as a red five-pointed star with coordinates (1.12,−16.93,−24.61) km. It can be found from the figure that the hypocenter depth has a significant impact on the error distribution.

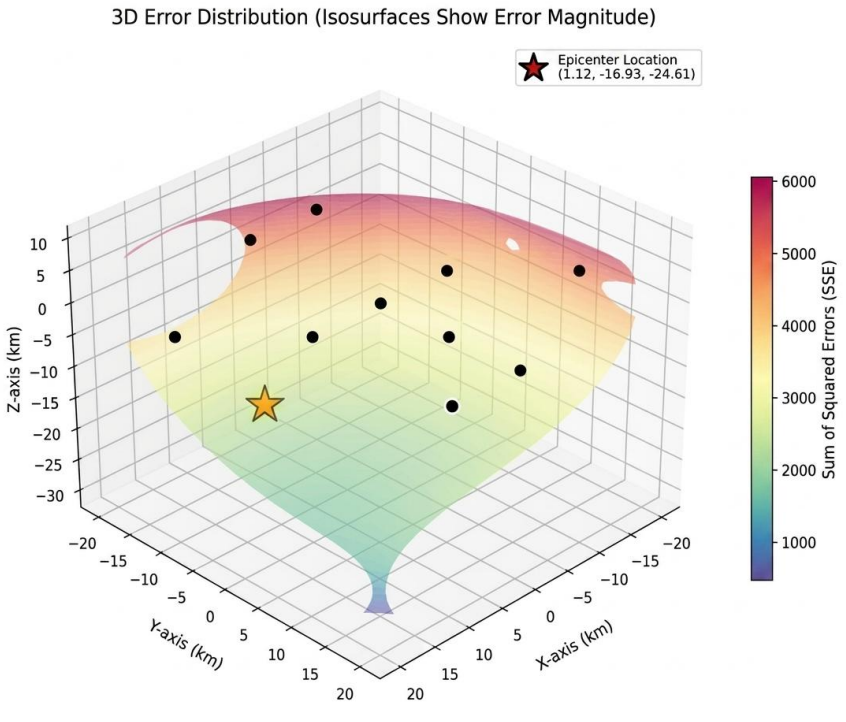

Figure 8 3D Error Distribution

3D error distribution is shown in Figure 8.

It can be seen from the figure that the influence of hypocenter depth on error distribution is reflected in the vertical direction. It can be seen from the figure that when the monitoring stations are located at different depths, the error distribution shows different characteristics. For example, in the area near the surface, the error is relatively large, while within a certain depth range, the error is significantly reduced. This indicates that reasonably setting the depth of monitoring stations can effectively reduce localization errors, especially when the hypocenter depth is large.

In this study, a numerical simulation method is used to systematically compare and analyze the influence of monitoring stations at the same depth (planar configuration) and different depths (three-dimensional configuration) on hypocenter localization accuracy, aiming to explore the mechanism of the spatial distribution of monitoring stations on seismic localization effects. The experimental design is based on extended monitoring station data, and two representative monitoring station layout schemes are constructed: one is a planar configuration (Flat Depth) where all monitoring stations are located on the same horizontal plane (Z=0); the other is a multi-depth configuration (Multi-Depth) where monitoring stations are distributed at five different depths of -5 km, -10 km, -15 km, -20 km, and -25 km. To comprehensively evaluate the influence of different configurations on localization accuracy, five sets of simulated hypocenter coordinates are generated in the study, covering different spatial locations and depth characteristics (see Figure 8), so as to reflect a variety of possible earthquake event scenarios.

Table 2 Simulated Hypocenter Coordinates

Hypocenter Number	X Coordinate (km)	Y Coordinate (km)	Z Coordinate (km)
S1	1.0	-15.0	-25.0
S2	2.0	-10.0	-20.0
S3	-3.0	-5.0	-30.0
S4	0.0	-12.0	-18.0
S5	5.0	-8.0	-22.0

Simulated hypocenter coordinates is shown in Table 2.

In terms of error model establishment, to be closer to the actual observation conditions, a random error of ±0.2% is introduced into the theoretical observation distance in this problem to simulate the uncertainty in the measurement process. At the same time, to ensure the fairness of the comparison, the same random seed is used for both configuration schemes to ensure the consistency of error distribution. Subsequently, in the implementation of the localization algorithm, the Nelder-Mead optimization algorithm is used to solve the hypocenter location, and the localization error is defined by the Euclidean distance:

$$\epsilon=\sqrt{(x_{est}-x_{true})^2+(y_{est}-y_{true})^2+(z_{est}-z_{true})^2} \tag{7}$$

where x_{est}, y_{est}, z_{est} represent the inverted hypocenter coordinates, and x_{true}, y_{true}, z_{true} represent the real simulated hypocenter coordinates.

On this basis, an evaluation index system is further constructed to quantify the difference in localization performance under the two monitoring station configurations. First, the localization error of each simulated hypocenter under each configuration is calculated, and the average value is taken as the measure of the overall localization error; second, the improvement percentage index η is defined to reflect the improvement range of the multi-depth configuration relative to the planar configuration:

$$\eta=\frac{\epsilon_{flat}-\epsilon_{multi}}{\epsilon_{flat}}\times 100\% \tag{8}$$

In addition, the error distribution characteristics in the three directions of x, y, and z are statistically analyzed to deeply analyze the constraint ability of different configurations on hypocenter localization in three-dimensional space.

According to the results shown in Figure 9, we observe that in all five simulated hypocenter locations (S1 to S5), the monitoring stations with different depth configurations significantly reduce the localization error compared with the same depth configuration. Specifically, the average localization error under the different depth configuration is significantly lower than that under the planar configuration, with an improvement percentage of 42.84%. For example, under the conditions of S1 and S3, the errors are reduced from 0.032 km and 0.035 km to 0.012 km and 0.016 km, respectively. This result indicates that optimizing the depth distribution of monitoring stations can greatly improve the accuracy of hypocenter localization. The conclusion drawn is that for the design and deployment of seismic monitoring networks, reasonably setting the depth of monitoring stations can not only effectively improve the accuracy of hypocenter localization but also show good adaptability in different hypocenter environments. This provides a clear answer to the question about how to evaluate the influence of different monitoring station configurations on hypocenter localization accuracy, that is, adopting a multi-level and three-dimensional monitoring station layout strategy is one of the key measures to improve the accuracy of seismic localization.

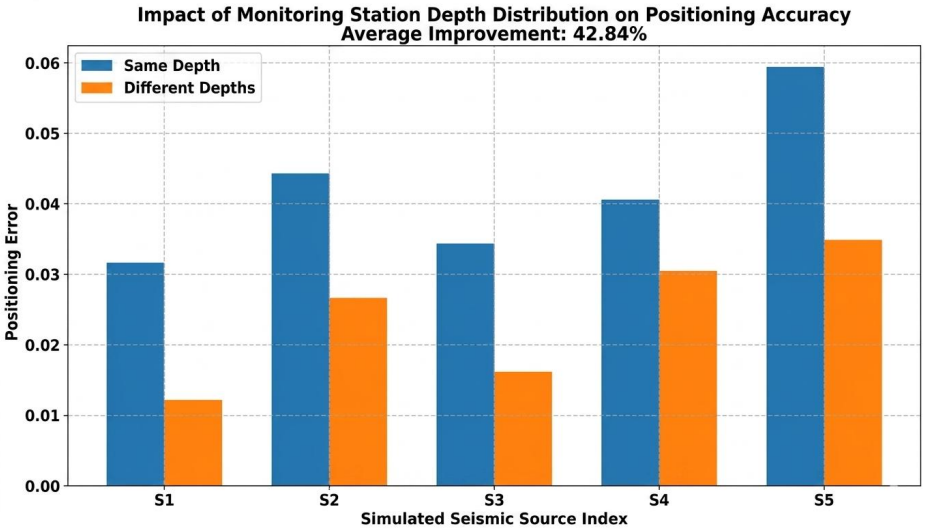

Figure 9 Influence of Monitoring Station Depth Distribution on Localization Accuracy

Influence of monitoring station depth distribution on localization accuracy is shown in Figure 9.

6 CONCLUSIONS

By establishing a complete technical chain of "theoretical modeling—error analysis—engineering optimization," this study systematically addressed the challenge of source localization ranging from ideal media to complex noise environments. The research confirmed that nonlinear optimization combining algebraic initial values with the Levenberg–Marquardt algorithm significantly enhances localization stability, while station network optimization based on the K-means approach and an outlier removal mechanism effectively resolved noise interference issues in multi-source data fusion. In particular, the proposed "three-dimensional station network" standard significantly reduces vertical localization errors through multi-depth configurations, providing data support for the upgrading of seismic monitoring systems. However, the current study still has certain limitations: the computational complexity of the nonlinear optimization algorithm reaches $O(n^3)$ under large-scale station networks, and real-time performance still needs optimization; furthermore, the single-source assumption limits its performance in scenarios involving signal aliasing from swarm earthquakes. Future research should focus on incorporating intelligent algorithms such as spatio-temporal graph neural networks (ST-GNN) to model the propagation characteristics of complex media, and on exploring GPU parallel computing architectures to improve localization timeliness, thereby providing more accurate decision-making support for earthquake early warning and resource exploration.

acquiring overseas advanced digital technologies as much as possible to feed back domestic enterprises,

COMPETING INTERESTS

The authors have no relevant financial or non-financial interests to disclose.

REFERENCES

[1] Wang C, Cao A, Jia B, et al. New Approaches to Assess Seismic Monitoring Quality in Underground Mines: Data Completeness and Source Location Accuracy. Applied Sciences, 2025, 15(21): 11559-11559.
[2] Liu S, Zhao J R, Lu H J, et al. High-precision identification and localization of noise sources based on acoustic metamaterials. Journal of Low Frequency Noise, Vibration and Active Control, 2025, 44(1): 274-289.
[3] He J, Li H, Li B, et al. Enhancing convergence speed and accuracy of virtual field optimization method for microseismic source location in tunnels. Tunnelling and Underground Space Technology incorporating Trenchless Technology Research, 2025: 158106366-106366.
[4] Feng Q, Han L, Ma L, et al. High-Precision Microseismic Source Localization Using a Fusion Network Combining Convolutional Neural Network and Transformer. Surveys in Geophysics, 2024, 45(5): 1527-1560.
[5] Zhang Q, Cheng Z, Liang H, et al. High-Precision Localization of Passive Intermodulation Source in Radio Frequency Transmission Lines Based on Dual-Frequency Signals. Electronics, 2024, 13(5).
[6] Chen X, Meng X, Gong Q, et al. High precision localisation of the sources of noise of a bent-axis motor. Vibration Worldwide, 2023, 54(7-8): 350-359.
[7] R D S, J R S, L. J H. Fracture-Mesh Faulting in the Swarm-Like 2020 Maacama Sequence Revealed by High-Precision Earthquake Detection, Location, and Focal Mechanisms. Geophysical Research Letters, 2023, 50(1).
[8] Lomax A, Savvaidis A. High-Precision Earthquake Location Using Source-Specific Station Terms and Inter-Event Waveform Similarity. Journal of Geophysical Research: Solid Earth, 2022, 127(1): e2021JB023190-e2021JB023190.
[9] Jian L, Feifei Z, Xiaoliang W, et al. The Underground Explosion Point Measurement Method Based on High-Precision Location of Energy Focus.IEEE ACCESS, 2020: 8165989-166002.
[10] Physics - Geophysics. New Findings from China Coal Research Institute Update Understanding of Geophysics (The Effect of P- and S-phase Arrivals On the Accuracy of Microseismic Source Location). News of Science, 2019.